Turkish Journal of Civil Engineering, 2025, xxxx-xxxx, Paper xxx, ***Research Article***

Intensity Characteristics of Seismograms Recorded During the February 6, 2023, M7.8 Türkiye Kahramanmaraş Pazarcik Earthquake

Kemal Onder CETIN[1*]
Alaa ELSAID[2]
A. Arda ÖZACAR[3]

ABSTRACT

The strong ground motion intensity levels recorded during the February 6, 2023, Türkiye-Kahramanmaraş-Pazarcık earthquake (M7.8) were compared with the ones predicted by the four ground motion models of 2014 NGA WEST-2 Ground Motion Prediction Equations (GMPEs), and by the Turkish earthquake design code (TEC, 2018). These comparisons revealed that Adana, Malatya, and Gaziantep cities were shaken by PGA levels less intense than the ones predicted by GMPEs. Contrary to these cities, ordered from the highest to lowest positive residuals, Şanlıurfa, Hatay, Kahramanmaraş, and Elazığ cities were shaken by higher levels of PGA than those predicted by the GMPEs. The TEC DD-1 and DD-2 seismic scenario PGA levels were exceeded at 5 and 22 out of 71 stations, respectively. The residuals for the stations on the Anatolian plate side exhibited a more correlated residual trend with the recorded PGA levels. The stations of exceeded seismic PGA demands are site class ZC or softer. PGA levels for DD-1 were exceeded at stations in the city of Hatay. The highest positive residual is also estimated for the Defne-Hatay station #3135, where the most structural damage was concentrated. The spectral acceleration residuals were also assessed. The spectral acceleration levels in all period ranges were higher than those predicted by Abrahamson, Silva and Kamai (2014), Campbell and Bozorgnia (2014) GMPE models. For spectral periods longer than 0.06 and 0.3 seconds, respectively, Chiou and Youngs (2014), and Boore, Stewart, Seyhan and Atkinson (2014) medial predictions were exceeded. Additionally, the structures with spectral periods of 0.7 seconds and longer were estimated to be subjected to approximately 20 to 30 % higher seismic demands, as defined by TEC for

Note:
- This paper was received on August 23, 2023 and accepted for publication by the Editorial Board on September 6, 2024.
- Discussions on this paper will be accepted by xxxxxxx xx, xxxx.

• https://doi.org/10.18400/tjce.1348206

1 Middle East Technical University, Department of Civil Engineering, Ankara, Türkiye
ocetin@metu.edu.tr - https://orcid.org/0000-0003-0540-2247

2 Middle East Technical University, Department of Civil Engineering, Ankara, Türkiye
elsd.alaa@gmail.com - https://orcid.org/0000-0003-0369-0417

3 Middle East Technical University, Department of Civil Engineering, Ankara, Türkiye
ozacar@metu.edu.tr - https://orcid.org/0000-0001-9700-4400

* Corresponding author

DD-2 design basis scenario. This is listed as one of the factors among many, contributing to the concentrated damage observed in residential buildings with number of stories higher than 5 to 7.

Keywords: Intensity, GMPEs, Turkish Earthquake code, Kahramanmaraş earthquake, Pazarcık earthquake.

INTRODUCTION

On February 6, 2023, two earthquakes, with moment magnitudes M7.8 and M7.6, occurred in southeastern Türkiye on the East Anatolian Fault Zone (EAFZ), at local times of 04:17 and 13:24, respectively. The induced damage scattered widely, affecting numerous provinces, including Kahramanmaraş, Gaziantep, Şanlıurfa, Diyarbakır, Adana, Adıyaman, Osmaniye, Hatay, Kilis, Malatya, and Elazığ, as shown in Figure 1.

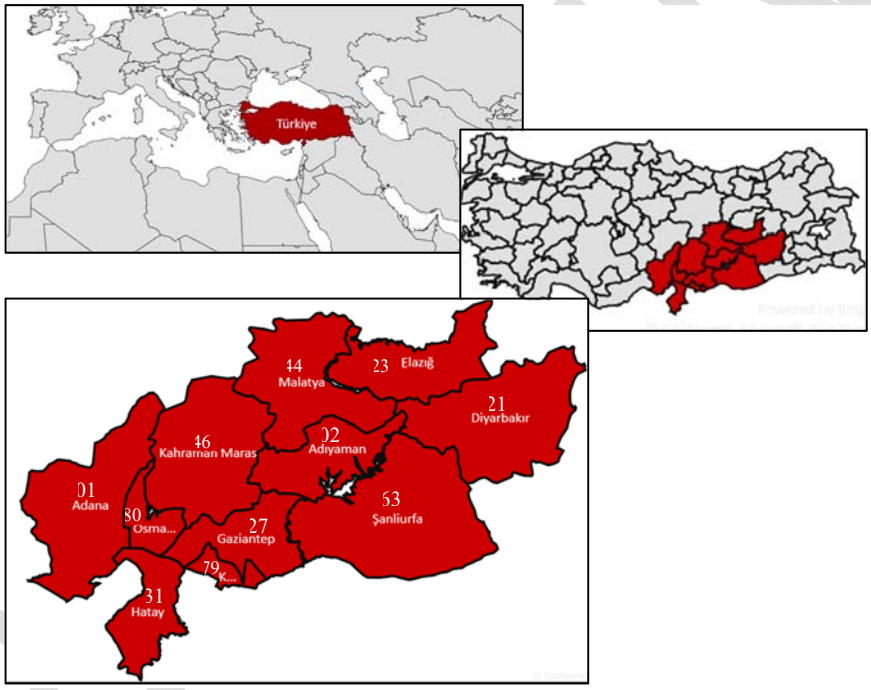

Figure 1 - The cities affected by the February 6, 2023, Türkiye-Kahramanmaraş-Pazarcık Earthquake M7.8

The resulting impact encompassed substantial casualties, injuries, and extensive infrastructure devastation. Referred to as the earthquake doublet, the cumulative effect of these events resulted in documented fatalities exceeding 50,000 in Türkiye, and 7,200 in Syria. Moreover, an estimated 15 million individuals were affected by these catastrophic events. The seismic activity also reportedly led to the destruction of around 520,000 residential units in Türkiye (Çetin et al., 2023a-b; Çetin and Ilgaç, 2023).

The second event occurred approximately 9 hours later at a focal depth of 7.0 km in Kahramanmaraş-Elbistan-Ekinözü, 100 km north of the first event's epicenter, on an east-west-striking northern strand of the EAFZ: more specifically on the Sürgü-Misis fault zone (SMFZ). Focal mechanism solutions offered by various agencies - AFAD (Disaster and Emergency Management Presidency), CMT (The Global Centroid-Moment-Tensor), USGS (United States Geological Survey), and GFZ (German Research Sciences for Geosciences) – consistently suggest strike-slip faulting as the prevailing source mechanisms for both events. This aligns harmoniously with both regional tectonics and the distinctive attributes of the EAFZ, on which both seismic events were located.

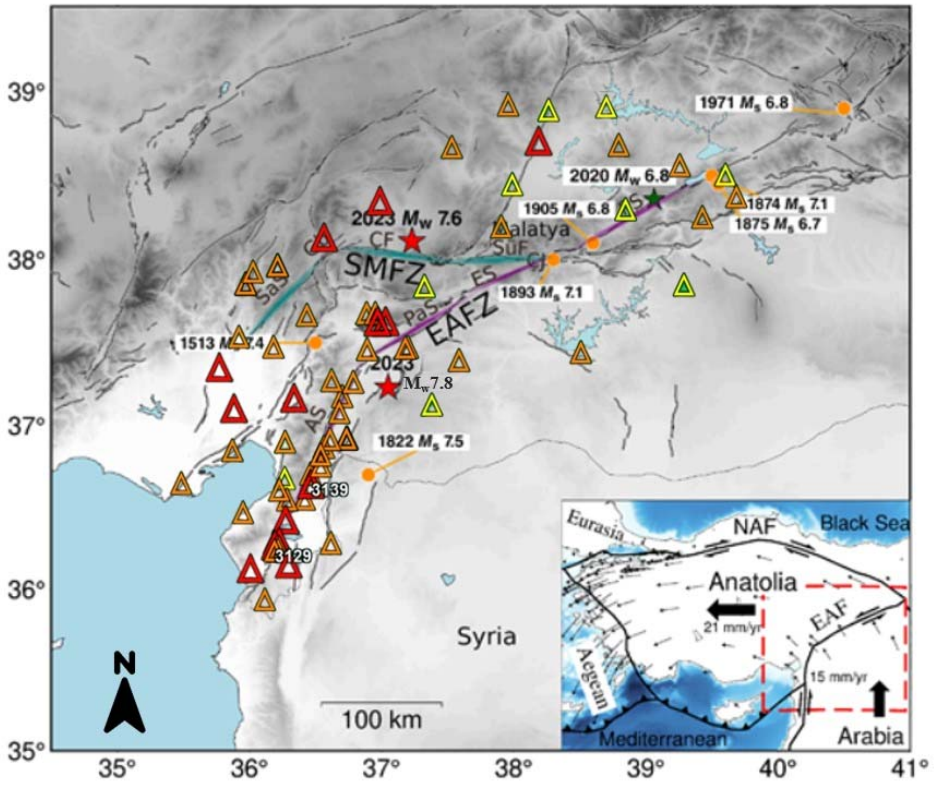

Figure 2 - Map of the region showing fault systems (Duman and Emre, 2013) and major historical earthquakes (orange circles; Ambraseys, 1989) along EAFZ. Kahramanmaraş-Pazarcık earthquake ruptured the main segments of the EAFZ (magenta) and Kahramanmaraş-Elbistan-Ekinözü earthquake ruptured the Sürgü-Misis fault zone (SMFZ; cyan). Red stars show epicenters of the events. EAFZ fault segments are labeled as AS, Amanos; Cj, Çelikhan junction; ES, Erkenek; PaS, Pazarcık;PS, Pütürge. SMFZ segments: CF, Çardak fault; Gb, Göksun bend; SaS, Savrun segment; and SüF, Sürgü fault (Duman and Emre, 2013). The triangles show the locations of the SGMSs: site class ZD: red, ZC: orange, ZB: yellow. The overview map provided in the lower right corner illustrates the main tectonic elements and their relative movement. Plate convergence rates are adopted from McClusky et al. (2000). The figure is adapted from Petersen et al. (2023).

As shown in Figure 2, the epicenter of the first event, which has a focal depth of 8.6 km, is in Kahramanmaraş-Pazarcık. Kahramanmaraş-Pazarcık earthquake initiated approximately 20 km southeast of the main strand of the EAFZ along a splay fault, more specifically along Narlı fault, which is oriented in the northeast-southwest direction (Melgar et al., 2023; Okuwaki et al., 2023, Petersen et al., 2023). The rupture nucleated on the splay fault propagated towards the north to the main strand of the EAFZ, rupturing a series of segments namely, Amanos, Pazarcık and Erkenek, during a multi-phased segmented rupture process (Okuwaki et al., 2023; Zahradník et al., 2023, Petersen et al., 2023). A series of elevated seismic activities were recorded in the region within a period of 10 months before the events (Kwiatek et al., 2023; Picozzi and Iaccarino, 2023). After the mainshock, more than 400 aftershocks with $M \geq 5$ were recorded in the period of February 6 to March 1, within 200 km radii of the epicenter.

STRONG GROUND MOTION DATA

Available strong ground motion records within 100 km from the fault rupture were accessed from Turkish Disaster and Emergency Management Authority (AFAD) web portal, accessible at https://tadas.afad.gov.tr (accessed August 2023). These strong ground motion records were already processed by AFAD. Given the methodological similarities between AFAD and NGA WEST-2 ground motion data processing protocols, additional signal processing was deemed unnecessary for comparison purposes. Both protocols encompass baseline correction, band-pass filtering, and time windowing to mitigate noise and enhance data integrity. While AFAD's protocol is tailored for regional specifics, it shares core principles with the ITACA protocol, including instrument response removal, baseline adjustment, and spectral filtering (Luzi et al., 2016). For more detailed information, please refer to the AFAD web portal (https://tadas.afad.gov.tr), the Italian Accelerometric Archive (ITACA) (Pacor et al., 2011; Massa et al., 2010), and the Engineering Strong-Motion Database (Luzi et al., 2016). The signal processing was performed in an automated manner, which was further adjusted manually when needed.

The strong ground motion stations (SGMSs), located within 100 km of the fault rupture plane ($R_{rup} \leq 100$ km) are shown in Figure 2. The stations outside this zone, or with invalid recordings, were excluded from further consideration, resulting to a total number of 71 stations in the database. The applicability/validity limits of GMPEs were checked. Only SGMS # 4404, which has a shear wave velocity measurement representing the upper 30 meters (i.e.: V_{s30}) value of 1380 m/s, violated the

ASK (Abrahamson, Silva and Kamai, 2014) $V_{s30}<1000$ m/s requirement. Hence it was excluded for the comparisons with ASK predictions. Among the remaining SGMSs, 51 of them have shear wave velocity (V_s) profiles, which are also accessible at https://tadas.afad.gov.tr. V_{s30} values range from 210 m/s to 1380 m/s. For the strong ground motion stations with missing values, V_{s30} were estimated based on V_{s30} model of Türkiye utilizing geology, topography, terrain and water saturation levels (Okay & Özacar, 2023). Table 1 provides a comprehensive summary of the employed strong ground motion station characteristics, encompassing essential parameters, including their coordinates, rupture distances, V_{s30} values, and the recorded peak ground acceleration (PGA) levels.

Table 1 - A summary of SGMS characteristics, and the recorded and predicted PGA levels (data accessed from AFAD web portal in August, 2023).

City	Station #	Longitude	Latitude	R_{rup} (km)	V_{s30} (m/s)	$PGA_{recorded}$ (g)			$PGA_{NGA\ WEST-2\ GMPE}$ (g)			PGA_{TEC} (g)		PGA recorded exceeded?	
						E-W	N-S	U-D	ASK	CB	CY	DD-1	DD-2	DD-1	DD-2
Adana	0119	35.39000	36.56800	83.8	485	0.045	0.044	0.026	0.078	0.075	0.084	0.633	0.310	No	No
	0120	35.79005	36.77006	59.6	439	0.118	0.115	0.105	0.114	0.103	0.118	0.778	0.356	No	No
	0122	35.82021	37.43390	86.1	501	0.053	0.058	0.034	0.075	0.072	0.081	0.601	0.315	No	No
	0125	35.79577	37.01519	69.8	216	0.085	0.131	0.036	0.121	0.100	0.128	0.506	0.331	No	No
	0127	35.92044	37.81618	95.8	583	0.052	0.056	0.040	0.062	0.061	0.068	0.555	0.283	No	No
	0130	35.67104	37.25186	90.3	358	0.070	0.083	0.036	0.081	0.073	0.088	0.519	0.326	No	No
	0131	36.11535	37.85660	84.7	631	0.163	0.149	0.051	0.069	0.070	0.074	0.599	0.306	No	No
	0132	36.11487	37.85589	84.7	631	0.033	0.039	0.030	0.069	0.070	0.074	0.600	0.306	No	No
	0133	35.86403	37.74550	96.3	631	0.076	0.079	0.040	0.060	0.059	0.065	0.591	0.298	No	No
	0134	35.86448	37.74427	96.2	631	0.047	0.070	0.039	0.060	0.059	0.065	0.592	0.299	No	No
Diyarbakır	2104	39.75900	38.26440	99.7	417	0.090	0.064	0.044	0.068	0.062	0.075	0.674	0.363	No	No
	2107	39.48379	38.14594	74.7	455	0.114	0.076	0.045	0.090	0.085	0.096	0.670	0.360	No	No
Elazığ	2302	39.67541	38.39231	95.6	907	0.224	0.201	0.112	0.051	0.054	0.054	0.786	0.413	No	No
	2308	39.31020	38.45063	68.9	450	0.167	0.329	0.408	0.098	0.091	0.103	1.326	0.722	No	No
	2309	38.72728	38.79913	74.2	860	0.036	0.038	0.026	0.069	0.074	0.071	0.460	0.229	No	No
	2310	38.82453	38.57266	51.4	426	0.052	0.062	0.050	0.130	0.116	0.135	0.792	0.412	No	No

Gaziantep	2703	37.35000	37.05800	51.4	758	0.163	0.153	0.082	0.104	0.103	0.105	0.394	0.214	No	No
Hatay	2708	36.64837	37.09933	4.0	523	1.111	0.828	0.996	0.474	0.477	0.546	1.232	0.610	No	Yes
	2711	37.56036	37.31736	35.2	555	0.099	0.109	0.063	0.160	0.148	0.165	0.356	0.208	No	No
	2712	36.73283	37.18400	1.0	599	0.614	0.566	0.350	0.543	0.537	0.635	1.144	0.562	No	Yes
	2715	36.68562	36.85536	9.8	468	0.347	0.466	0.078	0.353	0.349	0.411	1.028	0.534	No	No
	2716	36.68833	36.85643	10.0	431	0.233	0.260	0.168	0.353	0.344	0.414	1.023	0.531	No	No
	2717	36.69100	36.85548	10.3	455	0.120	0.141	0.082	0.346	0.340	0.403	1.018	0.528	No	No
	2718	36.62660	37.00777	1.7	421	0.656	0.716	0.596	0.534	0.499	0.651	1.257	0.635	No	Yes
	3115	36.16459	36.54634	19.1	424	0.215	0.280	0.219	0.256	0.237	0.286	0.685	0.362	No	No
	3116	36.20661	36.61618	18.7	868	0.169	0.164	0.166	0.203	0.223	0.219	0.522	0.276	No	No
	3123	36.15973	36.21423	14.4	470	0.606	0.668	0.885	0.292	0.282	0.334	1.013	0.501	No	Yes
	3124	36.17220	36.23870	11.7	283	0.650	0.584	0.589	0.333	0.301	0.391	0.826	0.448	No	Yes
	3125	36.13264	36.23808	14.6	448	1.145	0.839	1.158	0.293	0.280	0.335	0.967	0.482	Yes	Yes
	3126	36.13750	36.22020	15.4	350	1.049	1.234	1.091	0.295	0.269	0.338	0.830	0.448	Yes	Yes
	3129	36.13430	36.19117	17.9	447	1.223	1.394	0.842	0.263	0.246	0.295	1.042	0.511	Yes	Yes
	3131	36.16328	36.19121	16.2	567	0.346	0.356	0.147	0.262	0.260	0.292	1.040	0.511	No	No
	3132	36.17159	36.20673	14.4	377	0.524	0.525	0.361	0.302	0.281	0.349	1.017	0.504	No	Yes
	3133	36.57360	36.24320	27.9	471	0.146	0.223	0.089	0.198	0.181	0.211	0.822	0.405	No	No
	3134	36.20485	36.82763	28.2	374	0.208	0.251	0.143	0.208	0.183	0.224	0.609	0.332	No	No
	3135	35.88310	36.40886	36.4	460	1.394	0.755	0.601	0.166	0.149	0.173	0.540	0.300	Yes	Yes
	3136	36.24722	36.11593	21.6	344	0.402	0.544	0.225	0.248	0.219	0.274	0.712	0.418	No	Yes
	3137	36.48852	36.69293	1.0	688	0.859	0.461	0.509	0.525	0.543	0.604	1.303	0.666	No	No
	3138	36.51119	36.80262	2.0	618	0.761	0.906	1.089	0.520	0.526	0.588	1.332	0.678	No	Yes
	3139	36.41439	36.58383	0.3	272	0.514	0.588	0.386	0.499	0.442	0.661	1.028	0.516	No	Yes
	3140	35.94982	36.08155	38.3	210	0.223	0.198	0.180	0.186	0.150	0.196	0.744	0.424	No	No
	3141	36.21973	36.37260	6.9	338	0.869	0.963	0.631	0.408	0.385	0.489	0.838	0.449	Yes	Yes
	3142	36.36612	36.49797	0.4	539	0.761	0.660	0.513	0.555	0.533	0.682	1.180	0.581	No	Yes
	3143	36.55714	36.84891	0.4	445	0.358	0.389	0.420	0.555	0.515	0.705	1.394	0.699	No	No
	3144	36.48574	36.75691	2.1	535	0.779	0.623	0.461	0.525	0.516	0.611	1.345	0.685	No	Yes
	3145	36.40640	36.64536	3.7	533	0.710	0.611	0.673	0.482	0.485	0.553	1.282	0.644	No	Yes

	3146	36.22695	36.49076	11.5	439	0.353	0.491	0.347	0.331	0.321	0.385	0.945	0.471	No	No
Malatya	3147	36.06436	35.90236	48.8	558	0.048	0.058	0.030	0.124	0.115	0.126	0.851	0.439	No	No
	4404	38.87385	38.19588	22.3	1380	0.139	0.138	0.098	0.146	0.169	0.168	1.032	0.568	No	No
	4405	37.93960	38.81070	94.5	579	0.129	0.092	0.079	0.064	0.062	0.069	0.467	0.253	No	No
	4406	37.97378	38.34388	47.5	815	0.134	0.111	0.051	0.108	0.108	0.108	0.745	0.329	No	No
	4407	38.26406	38.78066	78.4	735	0.034	0.044	0.020	0.070	0.073	0.073	0.877	0.398	No	No
	4408	37.88732	38.09616	27.0	654	0.140	0.102	0.099	0.183	0.177	0.190	1.023	0.531	No	No
	4409	37.49076	38.56063	88.9	462	0.029	0.039	0.029	0.075	0.071	0.081	0.371	0.198	No	No
	4412	38.18385	38.59685	63.5	356	0.070	0.065	0.057	0.115	0.101	0.120	0.695	0.380	No	No
Kahramanmaraş	4611	37.28426	37.74720	18.5	731	0.327	0.356	0.177	0.221	0.231	0.240	0.819	0.430	No	No
	4612	36.48187	38.02395	79.7	246	0.125	0.144	0.055	0.104	0.090	0.111	0.601	0.344	No	No
	4613	36.35737	37.57010	48.8	434	0.157	0.150	0.076	0.135	0.120	0.139	0.658	0.334	No	No
	4615	37.13803	37.38676	10.3	484	0.592	0.595	0.677	0.343	0.341	0.398	1.000	0.514	No	Yes
	4616	36.83836	37.37547	2.3	390	0.516	0.627	0.406	0.518	0.483	0.629	1.047	0.530	No	Yes
	4617	36.83030	37.58551	22.2	574	0.117	0.148	0.113	0.217	0.209	0.233	0.717	0.374	No	No
	4620	36.89845	37.58568	19.3	484	0.327	0.306	0.189	0.247	0.234	0.274	0.778	0.407	No	No
	4624	36.91765	37.53610	13.7	280	0.326	0.364	0.165	0.312	0.279	0.362	0.774	0.441	No	No
	4625	36.98187	37.53872	11.1	346	0.494	0.457	0.374	0.342	0.319	0.403	0.861	0.470	No	Yes
	4628	36.92281	38.24120	81.9	337	0.084	0.093	0.057	0.092	0.083	0.099	0.480	0.306	No	No
	NAR	37.15740	37.39190	10.7	450	0.117	0.120	0.040	0.065	0.070	0.066	0.263	0.141	No	No
Şanlıurfa	6303	39.32910	37.75240	74.7	986	0.243	0.215	0.091	0.102	0.092	0.108	0.377	0.176	No	Yes
	6304	38.51316	37.36509	70.7	376	0.207	0.247	0.342	0.289	0.273	0.330	0.852	0.444	No	No
Osmaniye	8002	36.56195	37.19156	15.2	430	0.189	0.144	0.143	0.187	0.160	0.197	0.580	0.354	No	No
	8003	36.26936	37.08417	34.2	350	0.182	0.172	0.073	0.112	0.101	0.117	0.610	0.324	No	No
	8004	36.09763	37.37989	61.2	426	0.626	0.781	0.492	0.341	0.333	0.397	0.988	0.509	No	Yes

The seismic shaking levels recorded at SGMS #3139 and # 3129 are particularly important due to their proximity to the fault rupture plane. The locations of both stations are shown in Figure 2. SGMS # 3139, underlain by medium stiff soil layers with a shear wave velocity (V_{s30}) of 272 m/s, is in Kırıkhan-Hatay. It is 300 m away from the fault rupture plane (i.e.: R_{rup} =300 m), and is the nearest station, which provided a reliable set of seismograms. The recorded PGA values in the east-west (E-W), north-south (N-S), and vertical directions (U-D) are 0.584 g, 0.514 g, and 0.360 g, respectively. SGMS # 3129 is in Defne-Hatay, and recorded the highest PGA levels during this event. It is a medium stiff soil site with a V_{s30} value of 447 m/s. The recorded PGA values in the E-W, N-S, and U-D directions are 1.125 g, 1.138 g, and 0.731 g, respectively.

COMPARATIVE ASSESSMENT OF SEISMIC INTENSITY DEMAND LEVELS

In this section, the seismic intensity predictions by 2014 NGA WEST-2 Ground Motion Prediction Equations (GMPEs) are presented. More specifically, the predictions by ASK, CB (Campbell and Bozorgnia, 2014), CY (Chiou and Youngs, 2014), and BSSA (Boore, Stewart, Seyhan and Atkinson, 2014) models are compared with the recorded peak ground acceleration (PGA) and spectral acceleration (S_A) values. Similarly, the Turkish earthquake design code (TEC) basis intensities are comparatively presented. For comparison purposes, residual (error) plots are prepared, and the variation of residual terms are shown with respect to the i) station locations, ii) distance and angular orientation relative to the fault rupture plane, iii) V_{s30}, iv) recorded intensity levels.

Comparisons of the Recorded Vs. Predicted PGAs

PGA intensity levels are assessed by ASK, CB, CY and BSSA models. Then residuals are estimated for each ground motion station. The residuals (R_i) are defined as the difference between the natural logarithm of the recorded and predicted intensity measures (i.e.: IM_R and IM_{GMPE}), as given in Equation 1:

$$R_i = \ln(\mathrm{IM_i})_R - \ln(IM_i)_P \quad (1)$$

More specifically, in Equation 1, R_i represents the residual for station "*i*", and the $(IM_i)_R$ and $(IM_i)_P$ terms indicate the geometric mean of the recorded and predicted intensity measure at station *i*. These residuals are shown against Joyner-Boore distance (R_{jb}), V_{s30}, recorded PGA values, and the azimuth angle (θ). The azimuth angle (θ) is particularly selected to assess the rupture directivity and/or velocity effects.

It is important to acknowledge the role of supershear effects on ground motion characteristics. During a supershear rupture, the rupture front propagates faster than the shear wave velocity, and this can significantly amplify ground motion intensities, particularly in the fault-parallel direction. Hu et al. (2020) demonstrated that sustained supershear rupture tends to produce a clear Mach cone and amplified ground motion, especially in near-fault regions, with deeper hypocenter depths being more likely to sustain supershear rupture. Dunham & Archuleta (2004) highlighted how supershear transients, which were observed during the 2002 Denali earthquake, contributed to high ground motion intensities, particularly due to additional

Rayleigh waves along the fault surface. Bouchon et al. (2000) emphasized that such rupture dynamics, as observed in the 1999 Izmit earthquake, can lead to significantly enhanced ground shaking, especially in the direction of rupture propagation. Additionally, Song et al. (2008) found that supershear rupture impacts the amplitude and frequency content of ground motion, particularly at longer periods, which are critical for assessing seismic demand.

With the intent of assessing the directivity and supershear effects on strong ground motion records, the azimuth angle of each station is estimated. Consistent with Somerville et al. (1997), θ is defined as the azimuth angle between the fault plane and ray path, as illustrated in Figure 3. Since the rupture first initiated on a splay fault (i.e.: Narlı fault) in the southeast, then continued along the EAFZ bilaterally towards the north and south, the point where EAFZ changes strike forming a kink, is used as the modified epicenter for the calculation of azimuth angles. The kink point, and the modified epicenter is illustrated in Figure 3 (c). In our assessments we have assumed the distances for rupture and Joyner-Boore as identical (i.e.: $R_{rup} = R_{jb}$). This assumption holds for 90^o degree dipping fault rupture planes reaching the ground surface which were both satisfied during the Pazarcık event (Gülerce et al., 2023). Our assessments were performed on records obtained within 100 km of the fault rupture due to significantly reduced intensities (PGA < 0.02) and widely scattered data beyond it. This limitation should be considered when interpreting the results, particularly concerning event-specific anelastic attenuation effects.

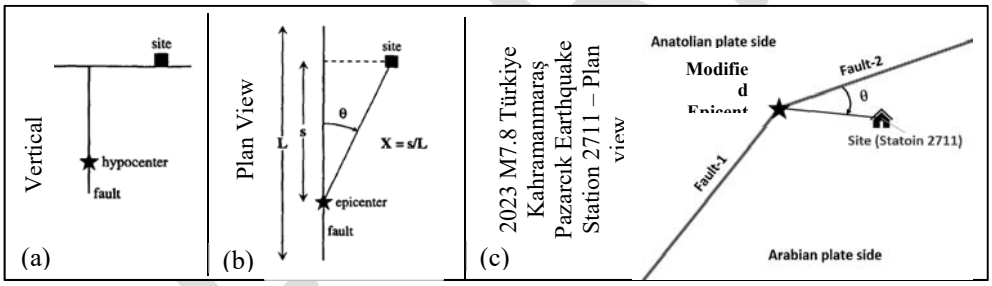

Figure 3 - Rupture directivity parameters for a strike-slip fault (after Somerville et al., 1997)

To assess possible path effects and the interaction between Arabian and Anatolian plates, SGMSs are binned as "on the eastern (on the Arabian plate)" and "on the western (on the Anatolian plate)" sides of the fault rupture. This allows to assess the dependency of residuals on SGMS's position relative to the causative plates.

Variability in PGA Residuals with Geographical Locations

The scatter in residuals is shown with respect to the geographical location of the stations. Figure 4 and Table 2 present the estimated residuals geographically grouped into city bins. On Figure 4, gray dashed lines show the mean, and mean plus and minus one standard deviation (σ) residuals estimated for the overall database. Similarly, mean, and mean ± σ residuals for each city bin, are shown in red solid lines. Circles and dots represent the

estimated mean residuals for the stations located on the Anatolian and Arabian plates, respectively. Table 2 presents a summary of the statistics of the residuals for each city.

The interpretation of Figure 4 and Table 2 reveals that Diyarbakır and Osmaniye cities had the most accurate predictions across all models, with the lowest mean residuals. For the other cities, the four GMPEs suggest that Adana, Malatya, and Gaziantep experienced PGA levels that were less intense than those predicted by them. In contrast, ordered from the highest to lowest positive residuals, Şanlıurfa, Hatay, Kahramanmaraş, and Elazığ were shaken by higher levels of PGA than those predicted by the GMPEs. Overall, Among the four GMPEs, the BSSA model provided the least biased predictions, producing the lowest overall mean residual. The overall mean ± σ residuals for the stations located east (Arabian plate side) and west (Anatolian plate side) of the fault rupture plane are estimated as 0.20 ± 0.66 and 0.14 ± 0.62, respectively. Hence, stations located on the Arabian plate side of the rupture demonstrate more pronounced overpredicted residuals, whereas those situated on the Anatolian plate side of the fault exhibit a slightly better fit with less overpredictions by these four models. The highest positive residual value is estimated for SGMS # 3135 in Hatay, where intense structural damage was reported.

The observed variability in ground motion data for Hatay can be attributed to a combination of site effects, including soil-site, basin, directivity and supershear effects, particularly those associated with the Amik Plain basin. The larger scatter in intensity recordings is also further influenced by the higher number of available Strong Ground Motion stations located on variable site conditions in Hatay. In contrast, Osmaniye exhibits a smaller spread, which can be attributed to under sampling of strong ground motion variability (i.e.: only two strong ground motion stations) or relatively homogeneous nature of geological setting.

Table 2 - A summary of mean ± σ residuals estimated for each city bin

City	ASK	CB	CY	BSSA
Şanlıurfa	0.70 ± 0.10	0.71 ± 0.19	0.66 ± 0.08	0.52 ± 0.06
Adana	-0.08 ± 0.39	-0.03 ± 0.39	-0.15 ± 0.39	-0.31 ± 0.4
Kahramanmaraş	0.21 ± 0.31	0.27 ± 0.29	0.10 ± 0.29	0.07 ± 0.32
Elazığ	0.21 ± 0.96	0.23 ± 0.94	0.16 ± 0.95	0.02 ± 0.95
Malatya	-0.25 ± 0.44	-0.24 ± 0.42	-0.31 ± 0.44	-0.40 ± 0.46
Hatay	0.42 ± 0.61	0.48 ± 0.62	0.29 ± 0.61	0.31 ± 0.6
Osmaniye	0.03 ± 0.31	0.13 ± 0.32	-0.04 ± 0.34	-0.13 ± 0.27
Gaziantep	-0.02 ± 0.50	0.00 ± 0.50	-0.15 ± 0.51	-0.13 ± 0.51
Diyarbakır	0.07 ± 0.04	0.14 ± 0.05	-0.01 ± 0.01	-0.18 ± 0.01
OVERALL	0.17 ± 0.58	0.22 ± 0.57	0.07 ± 0.57	0.02 ± 0.58

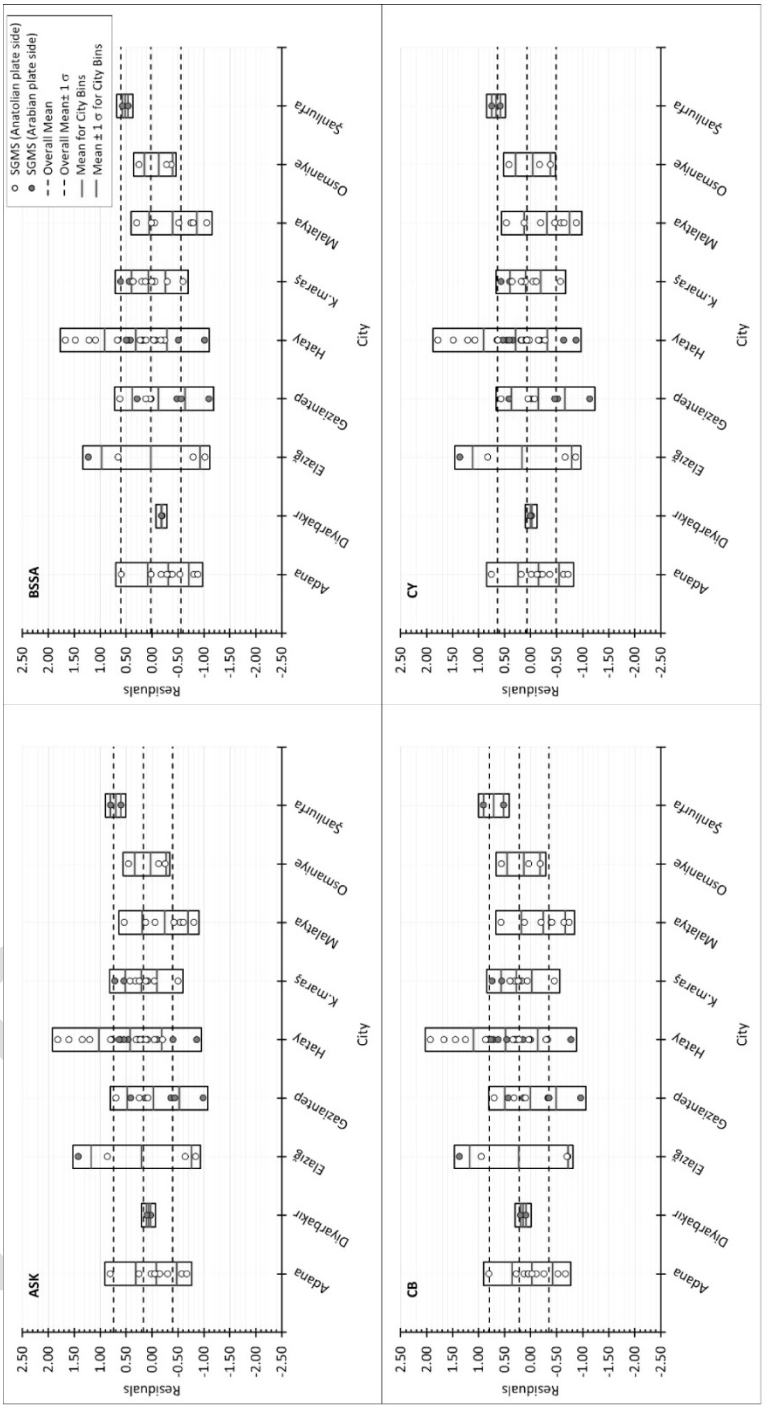

Figure 4 - PGA residuals estimated by the four GMPEs and their distribution with respect to the cities, where SGMSs are located.

Variability in PGA Residuals with Distances to the Rupture Plane

In Figure 5, PGA residuals are presented against R_{jb} .In Figure 5, SGMSs, located on the Anatolian and Arabian plate sides of the rupture, are shown by circles and dots, respectively. The trend lines for their residuals are shown by red and green lines, respectively. Table 3 presents a summary of mean ± σ residuals estimated separately for three R_{jb} bins: less than or equal to 10 km, in between 10 and 50 km, and greater than 50 km. Various bin thresholds were tested to identify meaningful trends in the data. After evaluating several options, these thresholds were selected due to their superior observed trends. These bins were also observed to be consistent with the distance attenuation response expected during a M7.8 event.

Table 3 - A summary of mean ± 1 σ residuals estimated separately for three different bins: i) $R_{jb} \leq$ 10 km, ii) < $R_{jb} \leq$ 50 km and iii) R_{jb} > 50 km

GMPE	$R_{jb} \leq$ 10 Km	10 km< $R_{jb} \leq$ 50 Km	R_{jb} > 50 Km
ASK	0.15 ± 0.43	0.29 ± 0.61	0.05 ± 0.57
CB	0.18 ± 0.42	0.35 ± 0.63	0.1 ± 0.57
CY	-0.02 ± 0.44	0.19 ± 0.6	-0.01 ± 0.57
BSSA	0.06 ± 0.43	0.18 ± 0.61	-0.17 ± 0.58

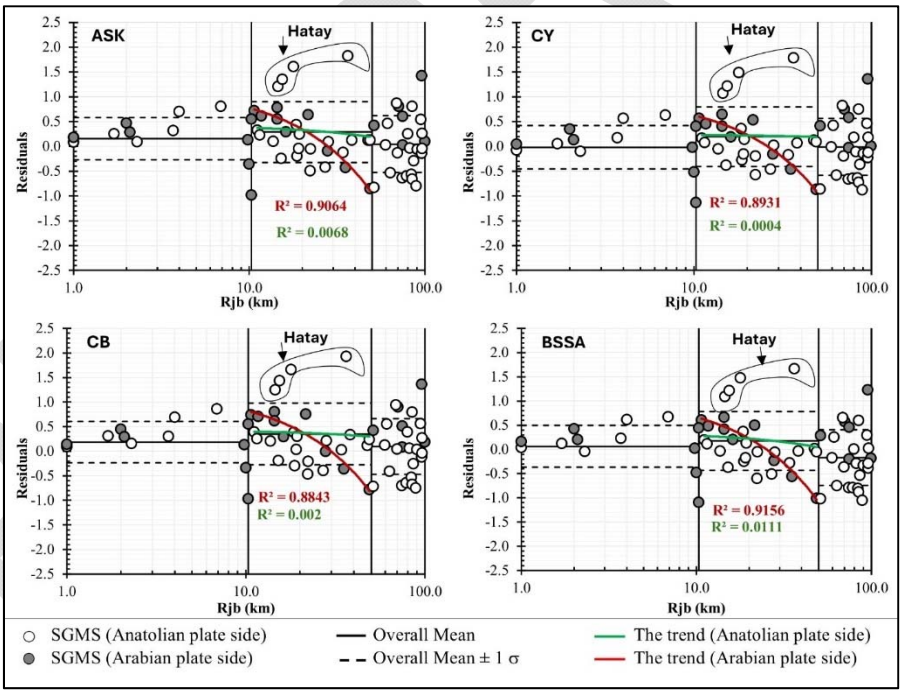

Figure 5 - PGA residuals for the four GMPEs and their distribution with respect to Rjb distances. The dashed lines in each plot show mean ± σ limits. Separated into three different bins: i) Rjb ≤ 10 km, ii) < Rjb ≤ 50 km and iii) Rjb > 50 km

Both Figure 5 and Table 3 reveal that the scatter in residuals increases for distances greater than 50 km, with a standard deviation around 0.6, indicating greater variability in predictions at longer distances. In contrast, distances less than 10 km show less scatter, with a standard deviation around 0.4, suggesting more consistent predictions close to the fault.

Additionally, the trend lines in Figure 5 show a strong decreasing trend in residuals with increasing R_{jb} for SGMSs on the Arabian plate side, particularly for stations located between 50 and 100 km. On the Anatolian plate side, the trend is very weak, with the highest residuals found at SGMSs stations 3135, 3129, 3126, and 3125, marked as outliers in Figure 5. These outliers are located in Hatay, where intense structural damage was observed. The differences in residual trends emphasize the significance of path effects on the recorded intensity levels.

Variability in PGA Residuals with V_{s30}

V_{s30} term is commonly used as a parameter to represent the effects of site response on the seismic demand levels. Figure 6 and Table 4 present the estimated residuals for each station grouped in terms of their V_{S30} values. On Figure 6, residuals are grouped into three bins, consistent with Turkish earthquake code-based soil site classifications scheme: ZB, ZC and ZD. It should be noted that TEC soil site classification scheme is almost identical with the one of NEHRP, and groups soil sites with $180 \leq V_{s30} < 360$, $360 \leq V_{s30} < 760$, and $760 \leq V_{s30} < 1500$ m/s, with site class symbols of ZD, ZC and ZB, respectively. Table 4 presents a summary of the statistics of the residuals estimated for each V_{S30} bin. Interpretation of Figure 6 and Table 4 reveals that the mean PGA residuals estimated by GMPES don't vary significantly with V_{S30}. The scatter (i.e.: standard deviation) in residuals is observed to be higher in stiffer sites ZC and ZB (i.e.: site class C and B in NEHRP), as compared to site class ZD.

Table 4 - A summary of mean ± 1 standard deviation residuals estimated separately for site class ZB, ZC and ZD by using NGA WEST-2 GMPEs

GMPE Model	$180 \leq V_{S30} < 360$ m/s ZD	$360 \leq V_{S30} < 760$ m/s ZC	$760 \leq V_{S30} < 1500$ m/s ZB
ASK	0.24 ± 0.46	0.15 ± 0.59	0.21 ± 0.66
CB	0.37 ± 0.44	0.19 ± 0.59	0.13 ± 0.67
CY	0.13 ± 0.44	0.05 ± 0.58	0.15 ± 0.66
BSSA	0.07 ± 0.49	0.00 ± 0.6.	0.11 ± 0.63

Variability in PGA Residuals with Azimuth Angle, θ

As discussed earlier, instead of the epicenter of the earthquake, the kink point of the fault rupture on the EAFZ, is used to assess the azimuth angle, θ, of the SGMSs. Figure 7 illustrates the dependency of the residuals on θ. An overall trend is evident across all GMPEs considered, wherein the residuals increase with decreasing θ angles. As the θ angle increases,

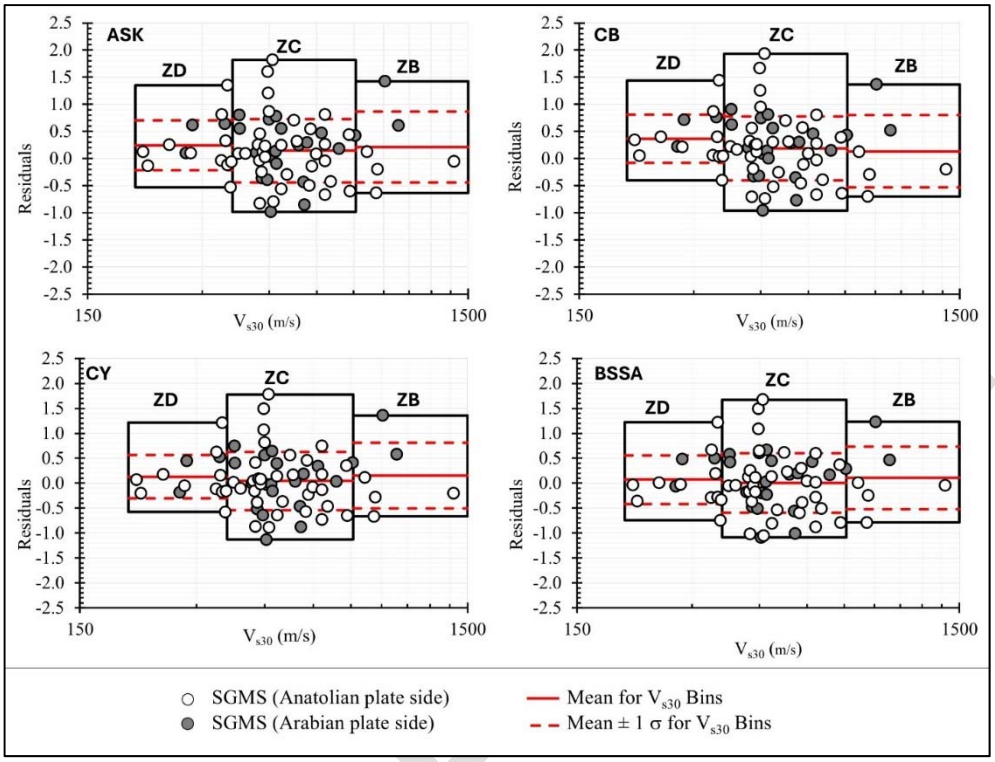

Figure 6 - PGA residuals for the NGA WEST-2 GMPEs, and their distributions with respect to VS30. The dashed lines in each plot show mean ± σ limits.

the scatter in residuals also decreases. In the literature, both directivity and rupture velocity (super vs. sub shear) effects are attempted to be represented by the azimuth angle between the fault plane and ray path rupture (Wang et al., 2016). Again, in the literature directivity effects are commonly accepted to affect longer period intensity levels but not PGAs (Somerville et al., 1997). Hence, the weak trend of PGA residuals increasing with decreasing θ is preliminarily attributed to rupture shear effects (speculated as super shear) as opposed to the directivity ones. However, this conclusion is premature and deserves further in-depth assessments, which is not within the scope of our preliminary reconnaissance evaluations.

Moreover, Supplementary Figures S.1 through S.4 provide a detailed geographical distribution of both the recorded PGA and the calculated residuals for each of the four GMP models. In these figures, the numbers shown at each SGMS represent the observed PGA value alongside the corresponding residual term, formatted as ($PGA_{recorded}$, $GMPE_{residual}$). This allows for a clear comparison between the recorded seismic activity and the predictions made by the ground motion models, highlighting areas where the models either underpredicted or overpredicted the actual ground motion.

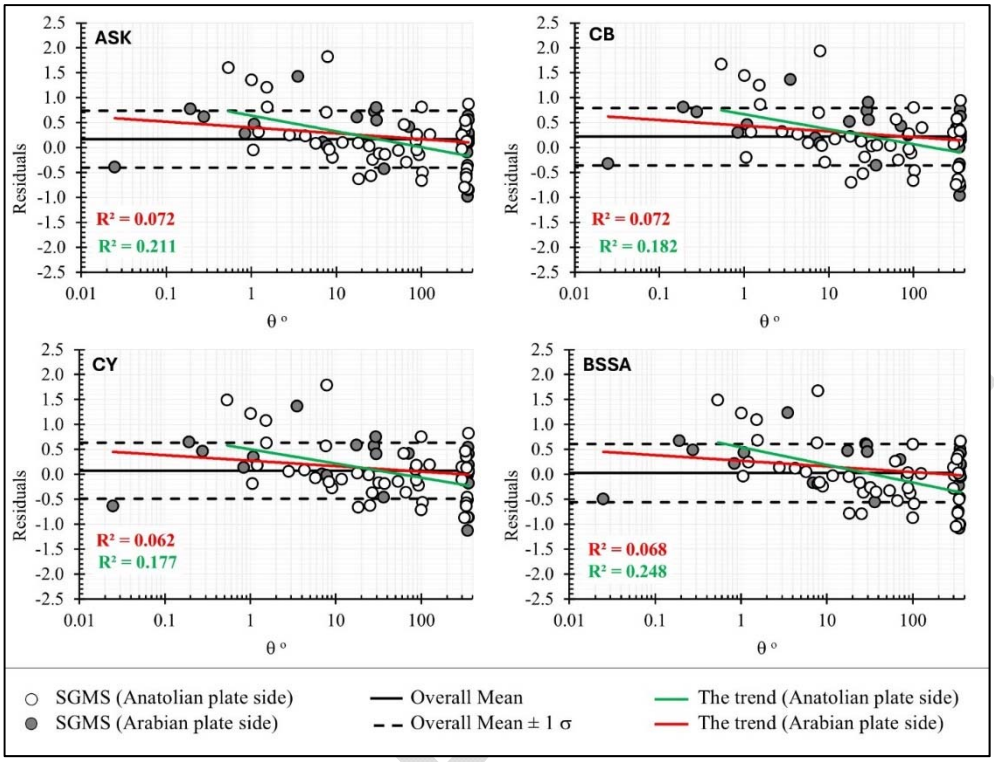

Figure 7 - PGA residuals for the NGA WEST-2 GMPEs, and their distribution with respect to ± σ The dashed lines in each plot show mean ± σ limits

Variability in PGA Residuals with Recorded PGAs

Figure 8 presents the estimated residuals varying with the recorded PGA levels. On the same figure the linear and nonlinear trends are shown separately for the stations located on the Anatolian and Arabian plate sides of the rupture. Valid for all four GMPE models, residuals increase with increasing recorded PGA levels. In simpler terms, the employed three GMPEs overpredicted lower PGA levels and underpredicted the higher ones. The residuals for the stations on the Anatolian plate side exhibited a more correlated residual trend with the recorded PGA intensity levels.

Comparisons of the Recorded Vs. Predicted S_A's

The spectral acceleration (S_A) residuals were assessed consistent with Equation 1. The scatter in residuals is shown with respect to spectral period, T, in Figure 9. On the figure, black solid lines show the mean values. As revealed by Figure 9, ASK consistently underestimated the spectral acceleration demand in all period ranges. CY and BSSA GMPE models underpredicted the spectral acceleration demand for period longer than 0.2 and 0.06 seconds,

respectively. CB GMP model has approximately residuals 0 up to a period of 0.06s afterward the model starts to underpredict the spectral acceleration. The underpredictions and overpredictions reach as high as 30 % in T=1 second in CY.

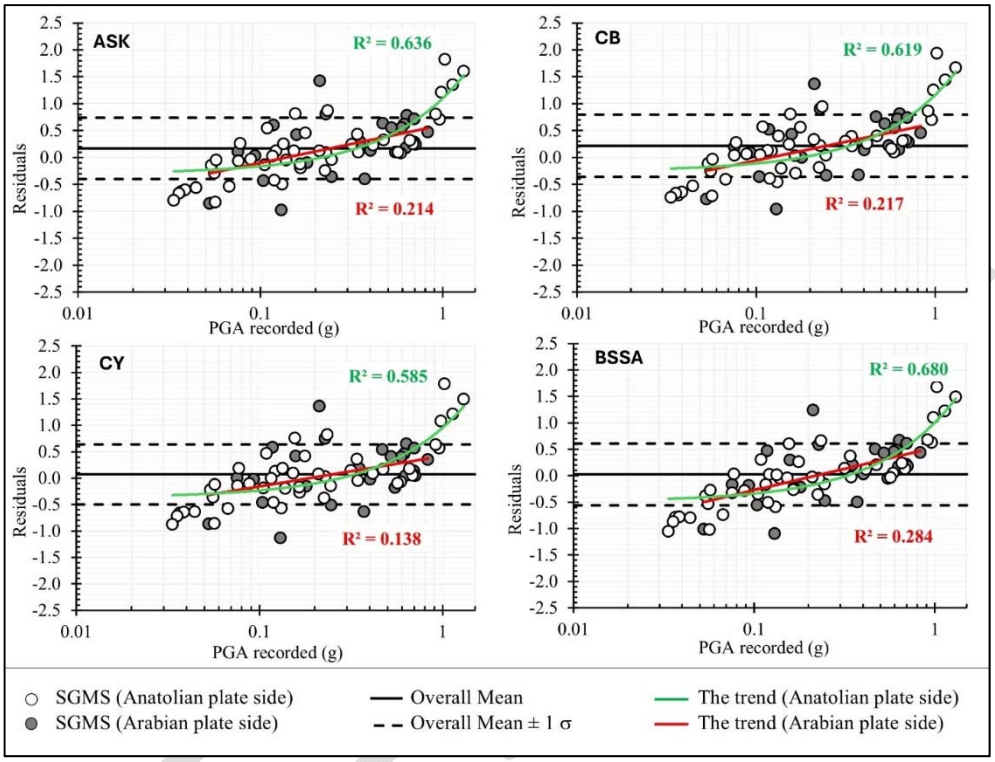

Figure 8 - PGA residuals for the NGA WEST-2 GMPEs and their distribution with respect to recorded PGAs. The dashed lines in each plot show mean ± σ limits

Comparisons of the Recorded vs. PGA and S_A Levels Recommended by Turkish Earthquake Code

Consistent with the Turkish Earthquake Design Code (TEC), the peak ground and spectral acceleration values were assessed for the design scenarios of DD-1 and DD-2, which correspond to the return periods of 2475 and 475 years, respectively. These values are compared with the recorded seismic demand levels at SGMS sites during the Kahramanmaraş-Pazarcık event. The results, as presented in Figure 10, and summarized in Table 2, reveal that the Turkish earthquake code DD-1 and DD-2 PGA levels were exceeded at 5 and 22, out of 71 stations, respectively. The exceedance of the design code could be attributed to site-specific conditions including soil-site, basin, directivity and rupture velocity effects, and the buildup of strain energies beyond design basis levels due to historical seismic gaps in the region. The stations, where the seismic PGA demand were exceeded, are class ZC or softer sites. PGA levels for the DD-1 seismic scenario were exceeded at SGMS # 3135,

3125, 3129, 3126, and 3141, which are all located in the city of Hatay. The extensive structural damage levels witnessed in this city consistently supports this conclusion (Çetin et al., 2023a; Çetin and Ilgaç, 2023). On the basis of the residual trends provided in Figure 11, structures with spectral periods of 0.7 seconds and longer, were subjected to approximately 20 to 30 % higher seismic demands than the ones defined by TEC for the DD-2 design basis scenario. This is listed as one of the factors among many, contributing to the concentrated damage observed in residential buildings with number of stories higher than 5 to7 (Çetin et al., 2023a; Çetin and Ilgaç, 2023). While comparisons of recorded PGA levels with design values provide some context for the concentrated damage, it is also important to note that a single parameter alone is not sufficient to fully assess complex structural seismic responses, which may require multi-dimensional evaluations and involvement of experts from different disciplines. In the literature S_A and peak ground velocity (PGV) are suggested as the parameters better correlating with seismic structural performance, as they offer a more comprehensive understanding of the damage mechanisms (Avcil et al., 2023; Pinzón et al., 2024).

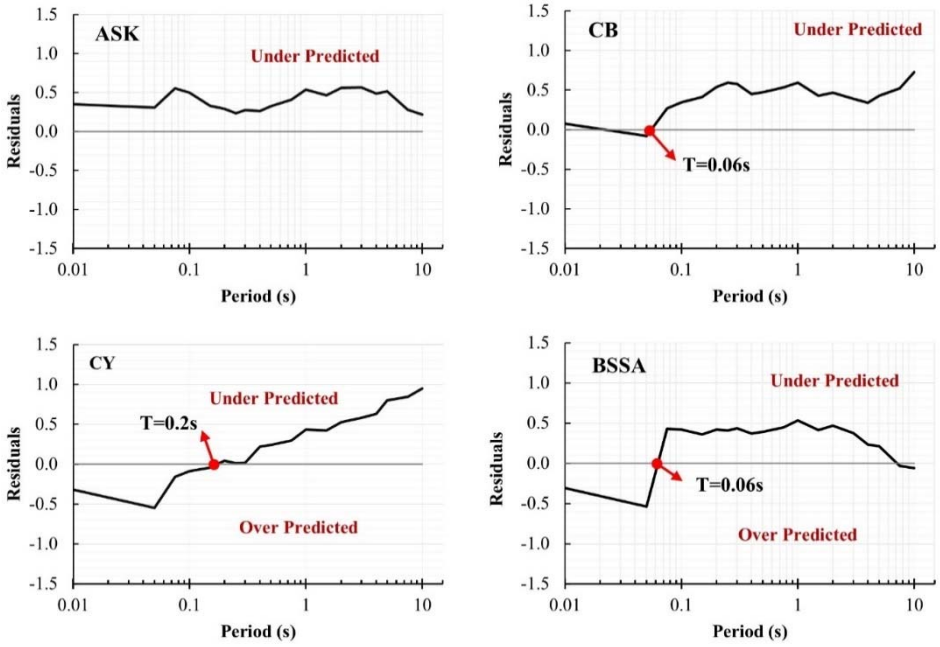

Figure 9 - SA residuals for the NGA WEST-2 GMPEs and their distribution with respect to spectral period (s).

Consistent with this discussion, Figure 11 represents the average spectral acceleration residuals of all stations calculated separately for each period. However, to provide a more detailed understanding, specific stations were selected for individual plotting on a detailed map, rather than averaging all SGMS spectral accelerations and comparing the average with the Turkish Earthquake Code. As mentioned earlier, several SGMS stations in Hatay were

identified as outliers, specifically stations 3135, 3125, 3129, and 3126, as shown in Figure 5. All of these stations are located on medium stiff soil, with shear wave velocities ranging from 350 m/s to 460 m/s. SGMS #3135 in Arsuz-Hatay recorded PGA values of 0.755 g (E-W), 0.601 g (N-S), and 0.166 g (U-D). SGMS #3125 in Antakya-Hatay recorded PGA values of 1.145 g (E-W), 0.839 g (N-S), and 1.158 g (U-D). SGMS #3129 in Defne-Hatay, which recorded the highest PGA levels during the event, reported values of 1.125 g (E-W), 1.138 g (N-S), and 0.731 g (U-D). SGMS #3126, also in Antakya-Hatay, recorded PGA values of 1.049 g (E-W), 1.234 g (N-S), and 1.091 g (U-D).

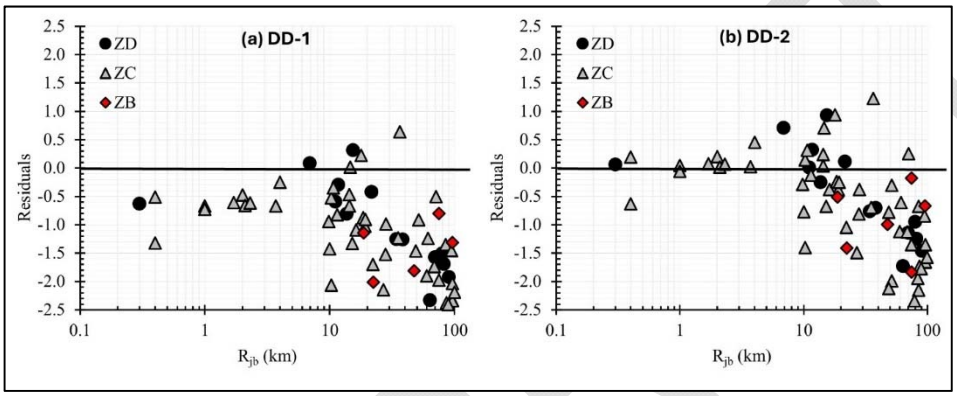

Figure 10 - PGA residuals estimated for the (a) TEC DD-1 (corresponds to a return period of 2475 years) and (b) TEC DD-2 (corresponds to a return period of 475 years) seismic scenario levels.

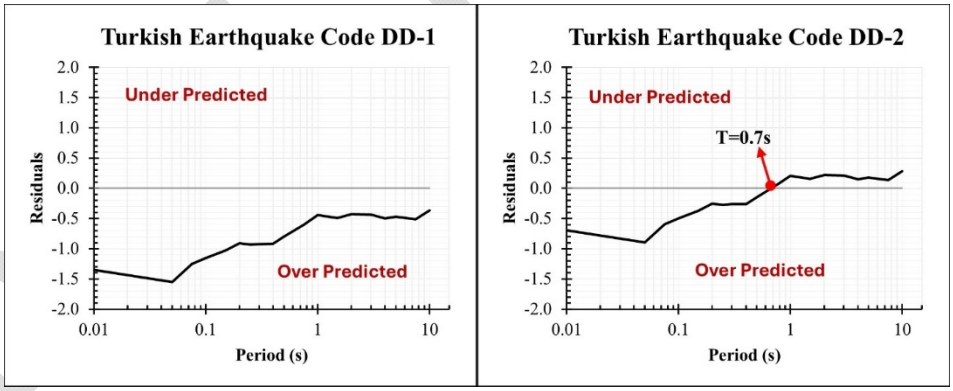

Figure 11 - SA residuals estimated for (a) TEC DD-1 (corresponds to a return period of 2475 years) and (b) TEC DD-2 (corresponds to a return period of 475 years) seismic scenario levels.

To better understand the underlying factors, elastic response spectra for these stations are shown in Figure 12. In this figure, the observed acceleration spectra are represented by solid

lines (black for the E-W spectral acceleration and red for the N-S), while the Turkish Earthquake Code spectra are indicated with blue dashed lines (DD-1 design-based scenario with a dashed line and DD-2 design-based scenario with a dash-dotted line). The map shows station locations with dots representing soil site class. It can be seen from the figure that at all four stations, the DD-2 design- based scenario was significantly exceeded. Notably, stations 3126 and 3129 exceeded the DD-1 scenario between the periods of 0.1-0.15 seconds, where the design spectra were approximately doubled. The significant deviations observed in these outlier stations underscore the influence of local site conditions and rupture dynamics on the seismic demands recorded in Hatay.

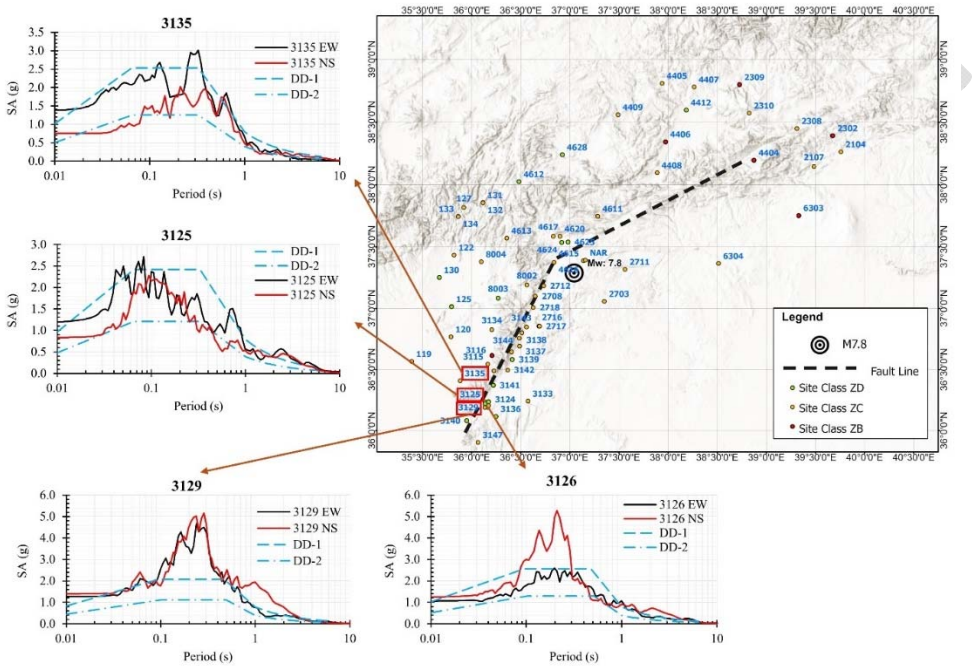

Figure 12 - Elastic response spectra for 3125, 3126, 3129 and 3135 SGM stations plotted on a map in relation to Turkish Earthquake Code.

SUMMARY AND CONCLUSION

This manuscript presents the findings of preliminary evaluations, which aim to comparatively assess the recorded spectral acceleration intensity levels during the February 6, 2023 Türkiye-Kahramanmaraş-Pazarcık earthquake, M7.8, with the ones i) predicted by four ground motion models from the 2014 NGA WEST-2 Ground Motion Prediction Equations (GMPEs): ASK, CB, CY, and BSSA.and ii) recommended by the Turkish earthquake design code (TEC) for return periods of 475 and 2475 years.

Across all models, the most accurate predictions were made for the cities of Diyarbakır and Osmaniye. The cities of Adana, Malatya, and Gaziantep were shaken by PGA levels less intense than those predicted by the GMPEs. Contrary to these cities, ordered from the highest

to lowest positive residuals, Şanlıurfa, Hatay, Kahramanmaraş, and Elazığ were shaken by higher levels of PGA than what were predicted by the GMPEs. In the overall, among others, BSSA model provided the least unbiased predictions, producing the lowest overall mean residual. The overall mean ± σ residuals for the stations located on the east (Arabic plate side) and west (Anatolian plate side) of the fault rupture plane are estimated as 0.20 ± 0.66 and 0.14 ± 0.62, respectively. Hence, stations located on the Arabian plate side of the rupture of the rupture are concluded to demonstrate more pronounced overpredicted residuals, whereas those situated on the Anatolian plate side of the fault exhibit a slightly better fit with less overprediction by the four GMPE models. The highest positive residual value is estimated for SGMS # 3135 in Hatay, where the most structural damage was concentrated.

The PGA residuals exhibited trends suggesting a strong decreasing trend in residuals with increasing R_{jb} for SGMSs on the Arabian plate side, particularly for stations located between 50 and 100 km. On the Anatolian plate side, the trend is very weak, with the highest residuals found at SGMSs stations 3135, 3129, 3126, and 3125, marked as outliers in Figure 5. These outliers are located in Hatay, where intense structural damage was observed.

In general, PGA residuals are observed to decrease with increasing rupture distances. The mean residuals among different GMPEs don't vary significantly with V_{S30}. The scatter (i.e.: standard deviation) in residuals, though, is observed to be the highest for site class ZC (i.e.: site class C in NEHRP). Valid for all four GMPE models, the PGA residuals increase with increasing recorded PGA levels. In simpler terms, the employed four GMPEs overpredicted lower PGA levels and underpredicted the higher ones. The residuals for the stations on the Anatolian plate side exhibited a more correlated residual trend with the recorded PGA levels. The dependency of the residuals on azitmuth angle, θ, was also assessed. An overall trend is evident across all GMPEs considered, wherein the residuals increase with lower θ angles, and as the θ angle increases, the residual PGAs decrease, and the scatter is reduced.

The spectral acceleration residuals were also assessed. The spectral acceleration demand across all period ranges was underestimated by ASK GMPE model. The CY and BSSA models provided underpredicted spectral intensities for periods longer than 0.2 and 0.06 seconds, respectively. The CB GMPE model had near-zero residuals up to 0.06 seconds, but underpredicted spectral acceleration values beyond it. The magnitude of underpredictions reach as high as 30 % at T=1 second for the predictions by CY.

The peak ground and spectral acceleration values were assessed for the Turkish earthquake code seismic scenarios of DD-1 and DD-2, which correspond to return periods of 2475 and 475 years, respectively. DD-1 and DD-2 PGA levels were exceeded at 5 and 22 out of 71 stations, respectively. The stations, where the seismic PGA demand was exceeded are all site class ZC or softer sites. PGA levels for the DD-1 seismic scenario were exceeded at stations 3135, 3125, 3129, 3126, and 3141, which are in all located in the city of Hatay. This is listed as one of the factors among many, contributing to the concentrated damage observed in Hatay city (Çetin et al., 2023a; Çetin and Ilgaç, 2023). While comparisons of recorded strong ground motion intensity levels with design values provide some context for assessing the observed damage levels, it is not sufficient to fully understand the underlying list of other factors. It is important to note that the structural seismic performance assessments require complex, multi-dimensional evaluations, and the involvement of engineering experts from a wide range of disciplines. Moreover, there may be other seismic demand parameters such as

PGV, which may correlate better with structural performance than PGA or S_A parameters. Hence, over-generalizations of our preliminary conclusions are discouraged.

Statement and Declarations

Acknowledgements

We would like to acknowledge the partial funding provided for the fieldwork by The Scientific and Technological Research Institution of Turkiye (TÜBİTAK) "1002-C Natural Disasters-Focused Fieldwork Emergency Support Program (Doğal Afetler Odaklı Saha Çalışması Acil Destek Programı)".

Funding: This work is partially supported by The Scientific and Technological Research Institution of Turkiye (TÜBİTAK) "1002-C Natural Disasters-Focused Fieldwork Emergency Support Program (Doğal Afetler Odaklı Saha Çalışması Acil Destek Programı)".

Competing Interests: The authors have no relevant financial or non-financial interests to disclose.

Author Contributions: Material preparation, data collection and analyses were performed by Kemal Önder Çetin and Alaa Elsaid and A. Arda Özacar. The manuscript was drafted by Kemal Önder Çetin, and Alaa Elsaid and A. Arda Özacar commented on the draft. All authors read and approved the final version of the manuscript.

Data availability: The datasets generated during and/or analyzed during the current study are available in the provided references and can also be provided by the corresponding author upon reasonable request.

References

[1] Abrahamson, N., and W. Silva (2008). Summary of the Abrahamson & Silva NGA Ground-Motion Relations, Earthquake Spectra 24, no. 1, 67–97, doi: 10.1193/1.2924360.

[2] AFAD - TADAS (n.d.): <https://tadas.afad.gov.tr>.

[3] Ambraseys, N. N. (1989). Temporary seismic quiescence: SE Turkey, *Geophysical Journal International* 96, no. 2, 311–331, doi: 10.1111/j.1365-246x.1989.tb04453.x.

[4] Avcil, F. et al. (2023) Effects of the February 6, 2023, Kahramanmaraş earthquake on structures in Kahramanmaraş City', Natural Hazards, 120(3), pp. 2953–2991. doi:10.1007/s11069-023-06314-1.

[5] Campbell, K. W., and Y. Bozorgnia (2023). Ground-motion model for the standardized version of cumulative absolute velocity, *Earthquake Spectra* 39, no. 1, 634–652, doi: 10.1177/87552930221144063.

[6] Chiou, B. S.-J., and R. R. Youngs (2014). Update of the Chiou and Youngs NGA Model for the Average Horizontal Component of Peak Ground Motion and Response Spectra, *Earthquake Spectra* 30, no. 3, 1117–1153, doi: 10.1193/072813eqs219m.

[7] Chiou, B., R. Darragh, N. Gregor, and W. Silva (2008). NGA Project Strong-Motion Database, *Earthquake Spectra* 24, no. 1, 23–44, doi: 10.1193/1.2894831.

[8] Çetin, K. Ö., M. Ilgaç , and E. Çakır (2023a). Preliminary Reconnaissance Report on February 6, 2023, Pazarcık Mw=7.7 and Elbistan Mw=7.6, Kahramanmaraş-Türkiye Earthquakes, METU/EERC 2023-01. doi: 10.13140/RG.2.2.32975.97446, Middle East Technical University Earthquake Engineering Research Center (METU EERC).

[9] Çetin, K. Ö., J. Bray , A. Frost , E. Miranda , R. Moss , and J. Stewart (2023b). February 6, 2023 Türkiye Earthquakes: Report on Geoscience and Engineering Impacts, https://10.18118/G6PM34, GEER Association Report 082.

[10] Çetin, K. Ö., and M. Ilgaç (2023). Reconnaissance Report on February 6, 2023 Kahramanmaraş-Pazarcık (Mw=7.7) and Elbistan (Mw=7.6) Earthquakes, 10.13140/RG.2.2.15569.61283/1., Türkiye Earthquake Reconnaissance and Research Alliance, Türkiye.

[11] Duman, T. Y., and Ö. Emre (2013). The East Anatolian Fault: geometry, segmentation and jog characteristics, *Geological Society, London, Special Publications* 372, no. 1, 495–529, doi: 10.1144/sp372.14.

[12] Kwiatek, G., P. Martínez-Garzón, D. Becker, G. Dresen, F. Cotton, G. Beroza, D. Acarel, S. Ergintav, and M. Bohnhoff (2023). Months-long preparation of the 2023 MW 7.8 kahramanmaraş earthquake, Türkiye, *Research Square preprint* , doi: 10.21203/rs.3.rs-2657873/v1.

[13] Massa, M., Pacor, F., Luzi, L., Bindi, D., Milana, G., Sabetta, F., Gorini, A., & Marcucci, S. (2010). The Italian Accelerometric Archive (ITACA): processing of strong-motion data. Bulletin of Earthquake Engineering, 8, 1175–1187. DOI: 10.1007/s10518-009-9152-3

[14] McClusky, S., S. Balassanian, A. Barka, C. Demir, S. Ergintav, I. Georgiev, O. Gurkan, M. Hamburger, K. Hurst, H. Kahle, *et al.* (2000). Global Positioning System constraints on plate kinematics and dynamics in the eastern Mediterranean and Caucasus, *Journal of Geophysical Research* 105, no. B3, 5695–5719, doi: 10.1029/1996jb900351.

[15] Melgar, D., T. Taymaz, A. Ganas, B. Crowell, T. Öcalan, M. Kahraman, V. Tsironi, S. Yolsal-Çevikbil, S. Valkaniotis, T. S. Irmak, *et al.* (2023). Sub- and super-shear ruptures during the 2023 Mw 7.8 and Mw 7.6 earthquake doublet in SE Türkiye, *Seismica* 2, no. 3, doi: 10.26443/seismica.v2i3.387.

[16] Luzi, L., Puglia, R., Russo, E., D'Amico, M., Felicetta, C., Pacor, F., Lanzano, G., Çeken, U., Clinton, J., Costa, G., Duni, L., Farzanegan, E., Gueguen, P., Ionescu, C., Kalogeras, I., Özener, H., Pesaresi, D., Sleeman, R., Strollo, A., & Zare, M. (2016). The Engineering Strong-Motion Database: A Platform to Access Pan-European Accelerometric Data. Bulletin of Earthquake Engineering.

[17] Okay, H. B., & Özacar, A. A. (2023). A Novel VS30 Prediction Strategy Taking Fluid Saturation into Account and a New VS30 Model of Türkiye. Bulletin of the Seismological Society of America, 114(2), 1048–1065. https://doi.org/10.1785/0120230032

[18] Okuwaki, R., Y. Yagi, T. Taymaz, and S. P. Hicks (2023). Multi-Scale Rupture Growth With Alternating Directions in a Complex Fault Network During the 2023 South-Eastern Türkiye and Syria Earthquake Doublet, *Geophysical Research Letters* 50, no. 12, doi: 10.1029/2023gl103480.

[19] Pacor, F., Paolucci, R., Luzi, L., Sabetta, F., Spinelli, A., Gorini, A., Nicoletti, M., Marcucci, S., Filippi, L., & Dolce, M. (2011). Overview of the Italian strong motion database ITACA 1.0. Bulletin of Earthquake Engineering, 9, 1723–1739. DOI: 10.1007/s10518-011-9327-6

[20] Petersen, G. M., P. Büyükakpinar, F. O. Vera Sanhueza, M. Metz, S. Cesca, K. Akbayram, J. Saul, and T. Dahm (2023). The 2023 Southeast Türkiye Seismic Sequence: Rupture of a Complex Fault Network, *The Seismic Record* 3, no. 2, 134–143, doi: 10.1785/0320230008.

[21] Picozzi, M., and A. Iaccarino (n.d.). The preparatory process of the 2023 MW 7.8 Turkey earthquake, *preprint*, doi: 10.21203/rs.3.rs-2619572/v1.

[22] Avcil, F. et al. (2023) Effects of the February 6, 2023, Kahramanmaraş earthquake on structures in Kahramanmaraş City, Natural Hazards, 120(3), pp. 2953–2991. doi:10.1007/s11069-023-06314-1.

[23] Somerville, P. G., N. F. Smith, R. W. Graves, and N. A. Abrahamson (1997). Modification of Empirical Strong Ground Motion Attenuation Relations to Include the Amplitude and Duration Effects of Rupture Directivity, *Seismological Research Letters* 68, no. 1, 199–222, doi: 10.1785/gssrl.68.1.199.

[24] Turkish Building Earthquake Code (2018), T.C. Resmi Gazete. , Ankara, Türkiye.

[25] Wang, D., J. Mori, and K. Koketsu (2016). Fast rupture propagation for large strike-slip earthquakes, *Earth and Planetary Science Letters* 440, 115–126, doi: 10.1016/j.epsl.2016.02.022.

[26] Zahradník, J., F. Turhan, E. Sokos, and F. Gallovič (2023). Asperitylike (segmented) structure of the 6 February 2023 Turkish earthquakes, *preprint*, doi: 10.31223/x5t666.